PAPER

Check for updates

A fast, reconfigurable flow switch for paper microfluidics based on selective wetting of folded paper actuator strips†

Taejoon Kong, [iD] ‡[a] Shawn Flanigan,‡[b] Matthew Weinstein,[a] Upender Kalwa, [iD] [a] Christopher Legner[a] and Santosh Pandey [iD] §*[a]

In paper microfluidics, the development of smart and versatile switches is critical for the regulation of fluid flow across multiple channels. Past approaches in creating switches are limited by long response times, large actuation fluid volumes, and use of external control circuitry. We seek to mitigate these difficulties through the development of a unique actuator device made entirely out of chromatography paper and incorporated with folds. Selective wetting of the fold with an actuation fluid, either at the crest or trough, serves to raise or lower the actuator's tip and thus engage or break the fluidic contact between channels. Here the actuator's response time is dramatically reduced (within two seconds from wetting) and a very small volume of actuation fluid is consumed (four microliters). Using this actuation principle, we implement six switch configurations which can be grouped as single-pole single-throw (normally OFF and normally ON) and single-pole double-throw (with single and double break). By employing six actuators in parallel, an autonomous colorimetric assay is built to detect the presence of three analytes – glucose, protein, and nitrite – in artificial saliva. Finally, this work brings the concept of origami to paper microfluidics where multiple-fold geometries can be exploited for programmable switching of fluidic connections.

Introduction

Paper-based device technology is an established sub-class of microfluidics[1–6] that aims to rival lateral flow test (LFT) assays[7–9] with their cheap costs, user friendliness, field-ready capability, and rapid time to result. A number of applications could immediately benefit from these field-deployable platforms, including those in healthcare,[10] environmental monitoring,[11] and food safety.[12,13] For instance, integrated paper-based platforms can be used to quickly detect food- and water-borne pathogens, early disease biomarkers from bodily fluids, and chemical contaminants or toxins in drinking water with the power to communicate the results wirelessly to related professionals.[1–6,10–15]

The scientific community has performed research in various areas of paper-based microfluidic technology, including device architectures, fabrication and printing methods, sur-

[a] *Department of Electrical and Computer Engineering, Iowa State University, Ames, IA 50011, USA. E-mail: pandey@iastate.edu*
[b] *Department of Mechanical Engineering, Iowa State University, Ames, IA 50011, USA*
† Electronic supplementary information (ESI) available. See DOI: 10.1039/c7lc00620a
‡ Joint first authors.
§ Address: 1050 Coover Hall, Department of Electrical and Computer Engineering, Iowa State University, Ames, IA 50011, U.S.A.

face functionalization schemes, fluid flow control strategies, application-specific protocols, readout instrumentation and mobile apps, and modelling of fluid transport and surface chemistry.[16–21] The driving force behind this rapid progress can be rightly attributed to the need for technology commercialization and widespread adoptability. While technology commercialization necessitates large volume production, low manufacturing costs, long shelf life and transportability, widespread adoptability requires customer satisfaction through easy-to-build and easy-to-use methodologies, faster testing times, digital readout, and reliable accuracy.[6,22] Just as LFT assays have created a billion-dollar industry in at-home pregnancy testing, there is scope for paper-based devices to capitalize the diagnostics market with ingenious fluidic toolkits and "killer applications" (*e.g.* for low-cost gene identification from environmental and clinical samples, multiplexed point-of-care screening of potential threat biomarkers).[23,24] A notable example of a paper-based microfluidic company is diagnostics for all (DFA) that has developed a range of capillary flow-based, colorimetric test platforms for use in resource-limited countries.[1–4]

To target commercially-viable applications, paper-based platforms should be able to handle multiple steps of an experiment, such as preparing samples, performing chemical tests, and detecting output signals.[25–34] Even though a range of expensive instruments are available today to perform the

steps in a diagnostic assay, a cheaper and all-integrated alternative in paper microfluidics could overcome the price barrier which is much needed in resource-limited settings. An important operation in realizing fully-functioning paper-based platforms is the regulation and switching of fluid flow in multiple channels.[26] The key metering parameters to regulate fluid flow in paper channels are: (i) fluid velocity, (ii) delay time, and (iii) switch configurations.[16]

Fluid velocity in a porous paper substrate can be regulated by manipulating parameters of the Lucas–Washburn flow equation, such as the medium porosity, fluid surface tension, fluid viscosity, and contact angle.[35,36] The geometric design (*i.e.* length and width) of porous channels can be altered to help speed up or slow down the advancement of fluid within the channels.[37,38] To achieve higher changes in fluid velocity within individual channels, the porous medium can be removed to create hollow channels with the incorporation of barriers or trenches in the fluid path to accelerate or impede the fluid flow.[39–41]

To regulate the *delay time of fluid flow* within a channel, fluidic delay timers have been realized by applying different concentrations[42] and colors of wax material[43] to the porous medium which modify the resistance or wettability of the channel and control the delay time. Another method to delay fluid flow involves the incorporation of dried dissolvable species (*e.g.* sucrose barriers) within the channel where the length of time delay is tunable and depends on the concentration of dissolvable species.[44] Delay in fluid flow can also be accomplished by placing absorbent shunt pads parallel to the porous medium where the material properties and physical dimensions of the shunt determine the delay time.[45]

The common *switch configurations* in paper microfluidics are 'normally OFF' and 'normally ON'. A 'normally OFF' switch (with no initial fluid flow) is actuated to permit fluid flow after a specific time while a 'normally ON' switch (with initial fluid flow) is actuated to block fluid flow after a finite time. User-activated, mechanical valves have been demonstrated in paper microfluidics to enable a 'normally OFF' channel to make contact with a reservoir (when desired by the user) and turn ON by the use of folding cards,[46] sliding action[47] or push buttons.[3] Autonomous valves have been shown where the hydrophobicity of a 'normally OFF' channel is altered to become hydrophilic and turn on by methods, such as polarization-based switching of an enclosed dielectric coating,[48] temperature-controlled manipulation of surfactant solubility,[49] corona discharge treatment of coated channels,[50] and melting of embedded wax barriers using on-chip heating elements.[51] On the other hand, fluid flow in a 'normally ON' channel can be switched off by using bridges composed of dissolvable material (*e.g.* sucrose, mannose or pullulan films)[52] or by physically lowering the relative height of the reservoir with respect to the channel's inlet.[53]

This work presents a novel valving concept for paper microfluidics where reversible switching between OFF and ON states is accomplished. The basic idea of using a paper-based device component both as a 'normally OFF' and 'nor-mally ON' switch has recently been presented in two publications.[26,54] In the first example,[54] a magnetic timing valve was fabricated by screen-printing silver ink electrodes on laser-cut paper strips and attaching a bridge of ferrous nanoparticle−PDMS blend. An ionic resistor triggered a power switch IC chip to activate an electromagnet and open/close the magnetic valve. Using the magnetic paper bridge, both 'normally ON' and 'normally OFF' switches were shown with a proof-of-concept demonstration of alkaline phosphate-based colorimetric reaction. One drawback of the magnetic timing valve is the need for an electromagnet and an electrical circuit (with power switch IC) which creates an extra cost burden. In the second example,[26] an actuator channel is made of high permeability glass fiber and the actuator is a compressed cellulose sponge adhered at the end of the actuator channel. The presence of actuation fluid causes expansion of the compressed sponge actuator that physically connects the input channel to the output channel. Three switch configurations have been demonstrated (*i.e.* 'normally OFF', 'normally ON', and diversion switches) along with control over the time for actuation and fluid flow volume by varying the wick lengths and size of absorbent pads, respectively. In this sponge actuation method,[26] there is scope to reduce the fluid absorption time by the sponge material (from 1.9 minutes) and volume of actuation fluid (from 500 μL).

Building on the above literature on switches for paper microfluidics and origami in paper-based devices,[55,56] we introduce an all-paper actuator that functions to reversibly control fluid flow from input channel(s) to output channel(s). The actuator is made entirely of chromatography paper − the same material used to make the flow channels. There are no external components adhered onto the paper actuator, unlike the previous examples of reversible switches which employ magnetic PDMS or sponge pads.[26,54] There is no external control circuitry or instrumentation to trigger the actuator. The actuator strip consists of uniquely-sized folds and is fastened at one end with tape. By dropping a small volume of fluid (∼4 μL) on the crest (or trough) of a fold, the actuator tip is raised (or lowered) to engage (or break) a physical contact between the input and output channels (Fig. 1a). Using this basic principle, we realized the following two switch configurations: single-pole single-throw (SPST) and single-pole double-throw (SPDT). The SPST and SPDT terminology is commonly used in the classification of commercial switches. The 'pole' refers to the number of inter-channel fluid connections being controlled by the actuator at a given time, while the 'throw' refers to the extreme (*i.e.* ON) position of the actuator. We show a SPST switch (similar to 'normally OFF' and 'normally ON' modes) that has one ON position and controls fluid flow across one inter-channel interface (Fig. 1b). The SPDT switches are also shown where two ON positions are possible and only one inter-channel interface is turned on at a given time. By actuating combinations of the fold's crests and troughs, four configurations of the SPDT switches have been realized (Fig. 1c and d). Lastly, a colorimetric assay is realized to detect the presence of three analytes − glucose, protein,
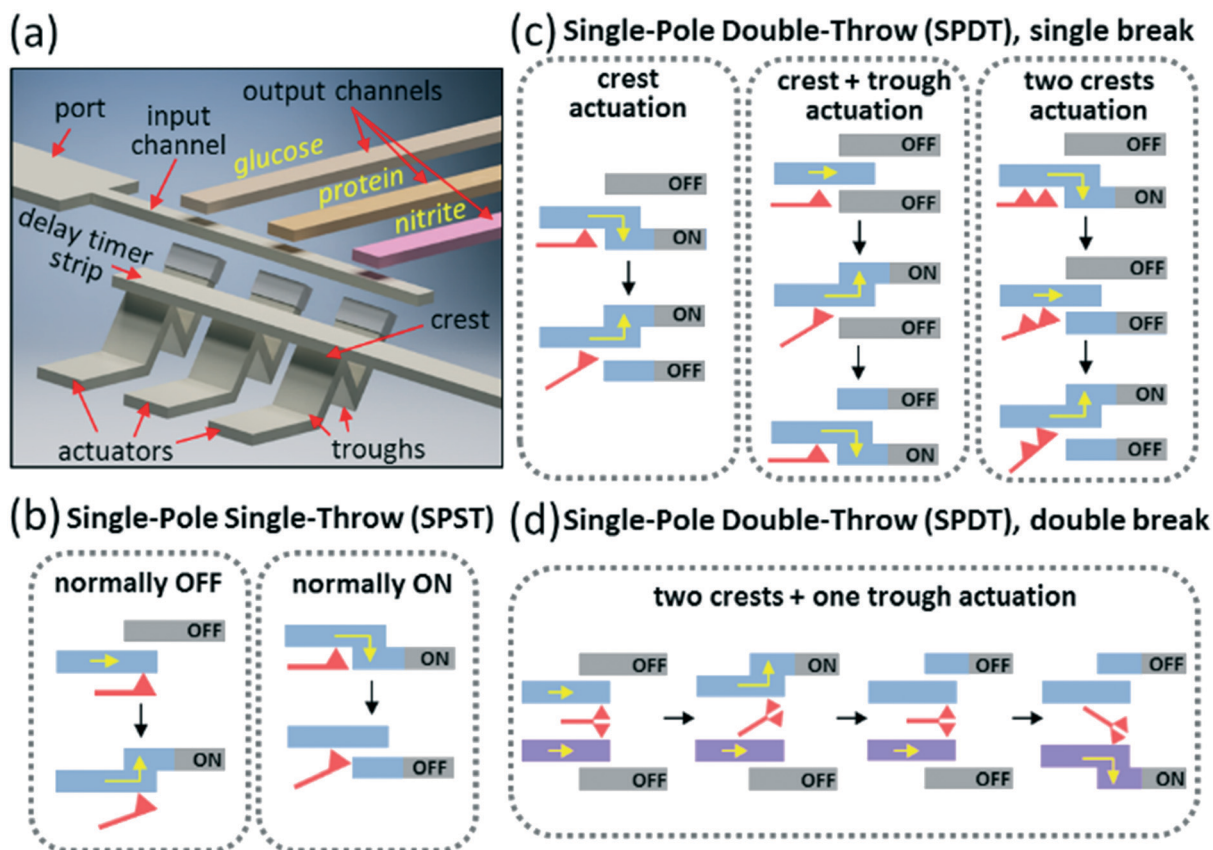
Fig. 1 All-paper actuator is presented where physical connection from the input channel to multiple output channels is established by activating the actuator. Water is added either directly on the folds or through a delay time strip to lift (or lower) the actuator tip. (a) CAD model of the actuator-controlled fluid flow is shown. Three actuators are activated by wetting their respective folds through a delay time strip. The output channels contain dried reagents to test the presence of glucose, protein, and nitrite in the test fluid applied at the port of the input channel. Upon activating the actuators, test fluid flows into the three output channels, and a color change occurs in the three output channels indicating the presence of the analytes. (b) Schematic of the single-pole single-throw (SPST) switch is shown. In the 'normally OFF' configuration, the output channel is initially separated by a vertical distance from the input channel and there is no fluid flow to the output channel. Upon activating the actuator, the input channel makes contact with the output channel and fluid flow is established. In the 'normally ON' configuration, both the input and output channels are in contact. Upon activating the actuator, the input channel is lifted and fluid flow is blocked to the output channel. (c) Schematic of the single-pole double-throw (SPDT), single-break switch is shown. Fluid flow from one input channel to two output channels is controlled by the actuator. The 'normally OFF' and 'normally ON' switches are combined together and the vertical position of the actuator tip is controlled by wetting the crest and/or trough of the actuator's fold. (d) Schematic of the single-pole double-throw (SPDT), double-break switch is shown. Fluid flow from two input channels to two output channels is controlled by the actuator. Fluidic connections to the two contacts are independently established by activating the crests and troughs of the actuator's fold.

and nitrite – in artificial saliva in an integrated platform. Control tests are run in parallel on the same platform. The assay is operated by six actuators which are activated by two delay timer paper strips and the time for actuation is automatically controlled by the wicking of actuation fluids.

Experimental

Materials and chemicals

200 mm × 200 mm sheets of chromatography paper (Whatman™, 1 CHR) are cut using a paper trimmer (Fiskars SureCut™) to form the flow channels, actuators and delay timer strips. Single-sided tape (Scotch™) is applied at the actuator tip to block any fluid flow from the channels to the ac-

tuator. A webcam (Logitech™) is used to image the fluid front in paper.

Artificial saliva is purchased from Pickering Laboratories™ (Monterey, CA) and pH test paper strips are purchased from Micro Essential Laboratory (Brooklyn, NY). The artificial saliva is spiked with 50 mM glucose, 200 μM BSA protein, and 2000 μM nitrite. Three different colorimetric assays are realized to detect the presence of glucose, nitrite and protein in the spiked artificial saliva samples. All chemicals for the colorimetric assay are purchased from Sigma Aldrich™. Experiments are conducted at room temperature (T = 22 °C).

Glucose assay. Phosphate buffer solution (PBS, pH = 6.0) is prepared by adding sodium phosphate dibasic heptahydrate (33 mg) and potassium phosphate monobasic anhydrous (105.25 mg) in distilled water (1 mL). The PBS is

stirred for 5 minutes. For every 1 mL of reagent solution, 120 units of glucose oxidase and 30 units of horseradish peroxidase are mixed into PBS. Once the two enzymes are mixed in PBS, 2.27 mg of trehalose is added that serves to stabilize the enzymes' performance and stability in the solution.[57] The dye chemical for the glucose assay is fulfilled with 99.6 mg ml^{-1} of potassium iodide and mixed for 10 minutes. For every cm^2 unit area of paper, 15 μL of the prepared reagent is applied to form the testing area. The chemical reaction is as follows: glucose is oxidized to δ-gluconolactone in the presence of glucose oxidase which is reduced to FADH$_2$ (reduced flavin adenine dinucleotide). Later, FADH$_2$ is re-oxidized to produce FAD and hydrogen peroxide. With horseradish peroxidase serving as a catalyst, the hydrogen peroxide reacts with the potassium iodide to produce a yellow-brown color.

Nitrite assay. A mixture of 69.3 mg mL^{-1} citric acid monohydrate is prepared in methanol. Then 8.61 mg mL^{-1} sulfanilamide (SA) and the dye chemical N-napthyl-ethylenediamine (NED) are added. The resultant solution is mixed for 10 minutes.[58] For every cm^2 unit area of paper, 15 μL of reagent is applied to form the testing area. The chemical reaction is as follows: nitrite is converted to nitrous acid in the presence of citric acid monohydrate and methanol. The resulting nitrous acid reacts with SA to form a diazo compound which turns colorless NED into a magenta color.

Protein assay. The priming solution and dye reagent solution are prepared separately and applied to the testing area.[59,60] The priming solution is formed by adding 51 mg mL^{-1} of 4.0 pH citrate buffer to a solution of 8% ethanol. To lower the pH of the solution to a more acidic level (i.e. 1.8 pH), 1300 μL of 1 M hydrochloric acid is added and the solution is mixed together for 5 minutes. For every cm^2 unit area of paper, 15 μL of priming solution is applied to form the testing area. The dye reagent solution consists of 8.87 mg mL^{-1} tetrabromophenol blue mixed into a solution of 95% ethanol. The resultant is mixed for 5 minutes. For every cm^2 unit area of paper, about 15 μL of dye reagent is applied to form the testing area. The chemical reaction is as follows: the acidic media causes tetrabromophenol blue to bind with protein in the sample. Ionic bonds form between the dye and protein, and the resulting complex creates a visible color change from orange to blue.

Design of the paper actuator

The chromatography paper is cut into 30 mm × 7 mm individual strips and each strip is folded into four pieces at spacing of 7.5 mm. A load (200 mg) is placed on the folded paper strips for 5 seconds. A single sided tape is applied at the tip of the paper strip to prevent any backflow of fluid from the channels. One end of the paper strip is physically taped to a flat surface. This forms a simple actuator, and further improvisations are possible (Fig. 1). Upon dropping a small volume of actuation fluid (i.e. water) on the crest of the folded section, the actuator is activated and its tip is raised. Conversely, wetting the trough of the folded section, the actuator tip is lowered. This principle is used to make or break the physical connection between an input channel (30 mm × 3 mm) and output channel (30 mm × 3 mm). The actuator's response time is within 1–2 seconds of wetting the crest or trough. Video files of the actuator device used in the different switch configurations are attached (video S1†).

Theoretical model of paper actuation

At the molecular level, the cellulose of the paper is organized into bundles of crystalline and amorphous orders. As water is dropped on the actuator's fold, the water molecules penetrate in between the hydrophilic cellulose fibers and form a network of hydrogen bonds at the water–cellulose interface.[61] A layered structure develops along the thickness of paper where the top surface is wet and the bottom surface is dry. This produces differential swelling causing the crease to relax and the fold angle to increase until the paper saturates with water.[62] The dynamics of relaxation at the fold can be modelled as a logarithmic two-step process with a quick, transient unfolding followed by a progressive, Arrhenius-like slow relaxation.[63]

We estimate of the actuation height achieved due to the wetting of the fold crease. A representative sketch of the actuator model is depicted in Fig. 2. A single fold comprises a crest and the two troughs as labelled in Fig. 2a. The left trough is taped in position while the rest of the actuator is free to move. The length of each side is L and the initial fold angle at the crest is 2θ (Fig. 2a). Upon wetting and activating the crest, the fold angle at the crest relaxes to 2α and the right trough is raised to a vertical height 'hC' given by eqn (1). The unfolding of paper at the crest is illustrated in Fig. 2b.

$$hC = 2L\sin(\alpha)\sin(\alpha - \theta) \qquad (1)$$

Upon wetting and activating the left trough, the initial fold angle at this trough (i.e. 90° + θ) relaxes to β and the right trough is lowered to a vertical height 'hT' given by eqn (2). The unfolding of paper at the left trough is shown in Fig. 2c.

$$hT = 2L\sin(\theta)\sin(\beta - \theta - 90) \qquad (2)$$

We measured the model parameters during two sets of experiments; crest activation and trough activation ($n = 4$ for each set using fresh actuators for each trial). The plane of the taped left trough is used as reference. The initial fold angle at the crest 2θ is 51° ± 2.5° and the initial fold angle at the left trough is 115° ± 2.9°. After dropping 4 μL of water on the crest to activate the actuator, the fold angle at the crest increases to 2α = 111.5° ± 1.7° and the right trough is raised to a height hC = 6.9 ± 0.5 mm. After wetting the left trough with 4 μL of water to activate the actuator, the fold angle at the trough increases to β = 153° ± 1.9° and the right trough is lowered to a height hT = 3.8 ±
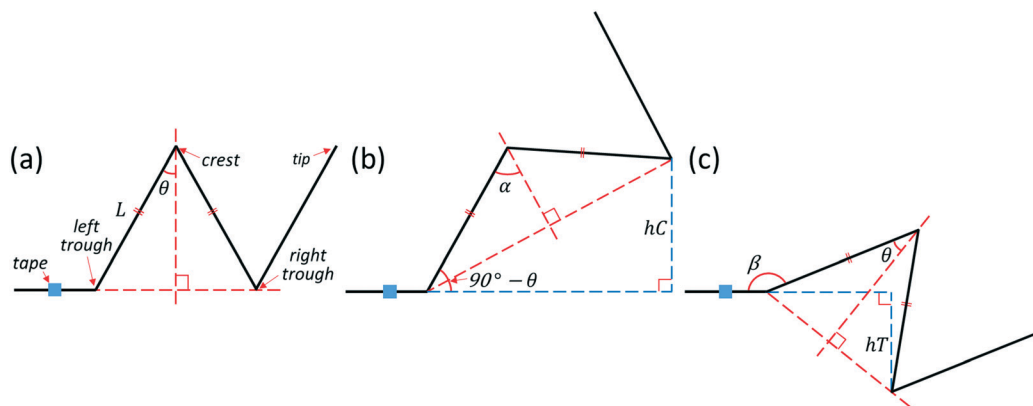
Fig. 2 Proposed actuation model to estimate the actuation height achieved by wetting the fold. (a) Initial position of the single-fold actuator is illustrated. The crest and the two troughs are labelled. The left trough is taped and rest of the paper is free to move. The length of each side is L. The initial fold angle at the crest is 2θ. (b) After crest activation, the fold angle at the crest relaxes to 2α and the right trough is raised to a height 'hC'. (c) After activating the left trough, the initial fold angle at this trough (*i.e.* $90° + \theta$) relaxes to β and the right trough is lowered to a height 'hT'. The expressions for the height raised (hC) and lowered (hT) are given by eqn (1) and (2), respectively.
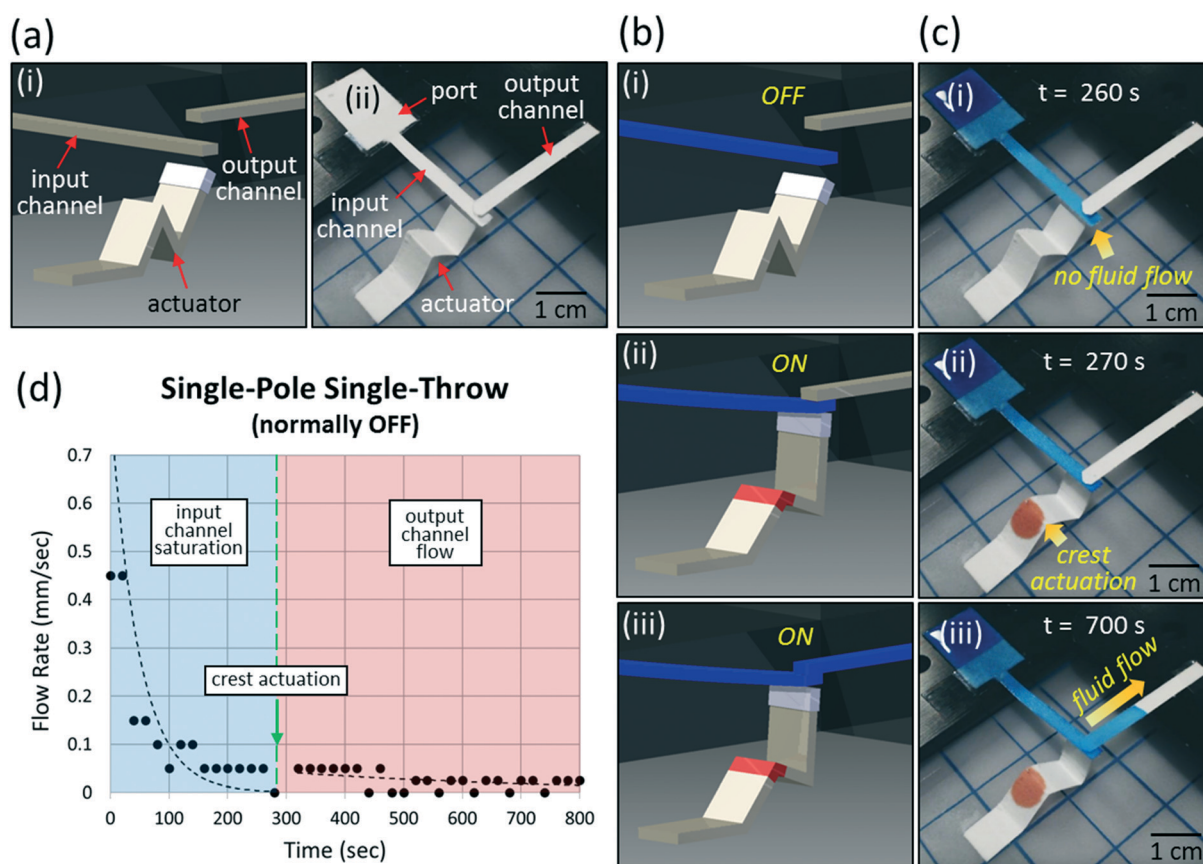

Fig. 3 Single-pole single-throw (SPST) 'normally OFF' switch. (a) CAD model (i) and actual image (ii) of the 'normally OFF' switch are shown. The input channel is separated by a vertical distance (2 mm) from the output channel. An actuator with a single fold is placed such that its tip is positioned vertically below the edge of the input channel. (b and c) Figures in panel (b) and panel (c) show the device in CAD model and actual experiment, respectively. Blue-colored water is dropped on the port of the input channel that eventually saturates it (b-i and c-i). No fluid flow is permitted in the output channel because of its physical separation from the input channel. Red-colored water is then dropped on the crest of the actuator's fold that raises the tip and brings the input channel in contact with the output channel (b-ii and c-ii). The blue-colored water now flows into the output channel (b-iii and c-iii). (d) Flow rate of the fluid front is plotted in the input channel before actuation and in the output channel after crest actuation.

0.2 mm. To check the validity of the proposed model, we calculated the two heights from eqn (1) and (2). Using $L =$ 7.5 mm, the values obtained from the theoretical model are: hC = 6.23 mm and hT = 3.93 mm.

Results and discussion

Single-pole single-throw (SPST) normally OFF switch

The device comprises two channels (input channel and output channel) that are initially separated by a vertical distance (2 mm) to prevent fluid flow between the two channels. An actuator with a single fold is placed vertically below (1 mm) the input channel. The CAD model and actual device are shown in Fig. 3a-i and Fig. 3a-ii, respectively. Upon activating the actuator, physical contact is established between two channels, thus allowing unrestricted fluid flow from the input channel to the output channel. The switching procedure is illustrated in the left panel (Fig. 3b, CAD model) and right panel (Fig. 3c, actual device). Around 225 μL of blue-colored water is dropped on the port of input channel. We found that this volume (*i.e.* 225 μL) is sufficient to saturate the input channel. Through wicking, the input channel absorbs the blue-colored water until it is saturated with the liquid (Fig. 3b-i and c-i). No fluid flow is permitted in the output channel because of its physical separation from the input channel. This configuration represents the OFF state of the

device. To switch the state of the device, 4 μL of red-colored water is dropped on the crest of actuator's fold. This raises the actuator tip that, in turn, lifts the edge of the input channel to make contact with the output channel (Fig. 3b-ii and c-ii). The volume of actuation fluid used here (*i.e.* 4 μL) is sufficient to selectively wet the chosen crest without wetting the adjacent troughs. Thereafter, the blue-colored water flows from the input channel to the output channel (Fig. 3b-iii and c-iii). This configuration represents the ON state of the device. Because the top surface of the actuator tip is protected with tape, there is no observable cross-contamination between the red-colored actuation fluid and blue-colored sample fluid. This is an advantage over magnetic timing valves[54] and sponge actuators.[26] The flow rate of fluid front in the two channels is imaged and plotted in Fig. 3d.

Single-pole single-throw (SPST) normally ON switch

The device comprises two channels (input channel and output channel) that are initially in physical contact, thereby
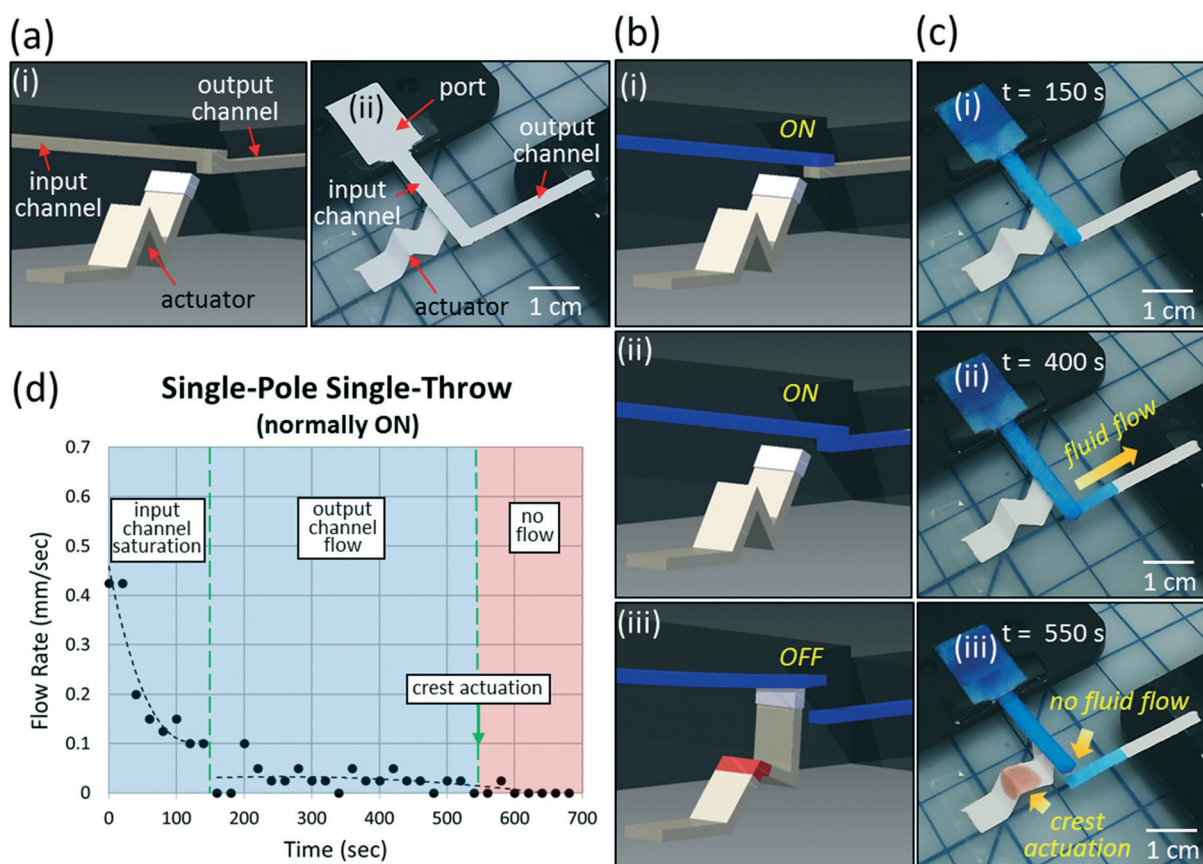

Fig. 4 Single-pole single-throw (SPST) 'normally ON' switch. (a) CAD model (i) and actual image (ii) of the switch are shown. Initially, the input channel is in contact with the output channel and fluid flow occurs between the two channels. An actuator with a single fold is placed such that its tip is positioned vertically below the input channel. (b and c) Figures in panel (b) and panel (c) show the device in CAD model and actual experiment, respectively. Blue-colored water is dropped on the port of the input channel that eventually saturates it (b-i and c-i). Fluid flow is permitted to the output channel (b-ii and c-ii). Red-colored water is then dropped on the crest of the actuator's fold that raises the tip of the actuator and lifts the input channel to physically separate from the output channel. (b-iii and c-iii). (d) Flow rate of the fluid front is plotted in the input and output channels before actuation and in the output channel after crest actuation.

allowing unrestricted fluid flow from the input to the output channel. An actuator with a single fold is placed vertically below (1 mm) the input channel. The CAD model and actual device are shown in Fig. 4a-ia and a-ii, respectively. Upon activating the actuator, the tip of the input channel is lifted and physically separated (1 mm) from the output channel. This prevents any further fluid flow from the input channel to the output channel. The switching procedure is illustrated in the left panel (Fig. 4b, CAD model) and right panel (Fig. 4c, actual device). Around 225 μL of blue-colored water is dropped on the port of input channel. Through wicking, the input channel absorbs the blue-colored water until it is saturated with the liquid (Fig. 4b-i and c-i). The fluid now flows into the output channel because of the physical contact between the two channels (Fig. 4b-ii and c-ii). This configuration represents the ON state of the device. To activate the actuator, 4 μL of red-colored water is dropped on the crest of actuator's fold. The actuator tip is raised vertically that subsequently lifts the edge of the input channel. A physical separation (1 mm) is created between the two channels that inhibit any

fluid flow from the input channel to the output channel (Fig. 4b-iii and c-iii). The flow rate of fluid front in the two channels is imaged and plotted in Fig. 4d.

Single-pole double-throw (SPDT), single-break switch

Crest actuation of a single-fold actuator. The device comprises three channels (input channel and two output channels). Initially, the input channel is in physical contact with output channel 1, thereby allowing unrestricted fluid flow from the input to the output channel 1. Output channel 2 is vertically separated (2 mm) from the input channel. An actuator with a single fold is placed vertically below (1 mm) the input channel. The CAD model and actual device are shown in Fig. 5a-ia and a-ii, respectively. Upon activating the actuator, the tip of the input channel is lifted to separate from output channel 1 and make contact with output channel 2. This switches the input channel's fluid flow from output channel 1 to output channel 2. The switching procedure is illustrated in the left panel (Fig. 5b, CAD model) and right panel (Fig. 5c,
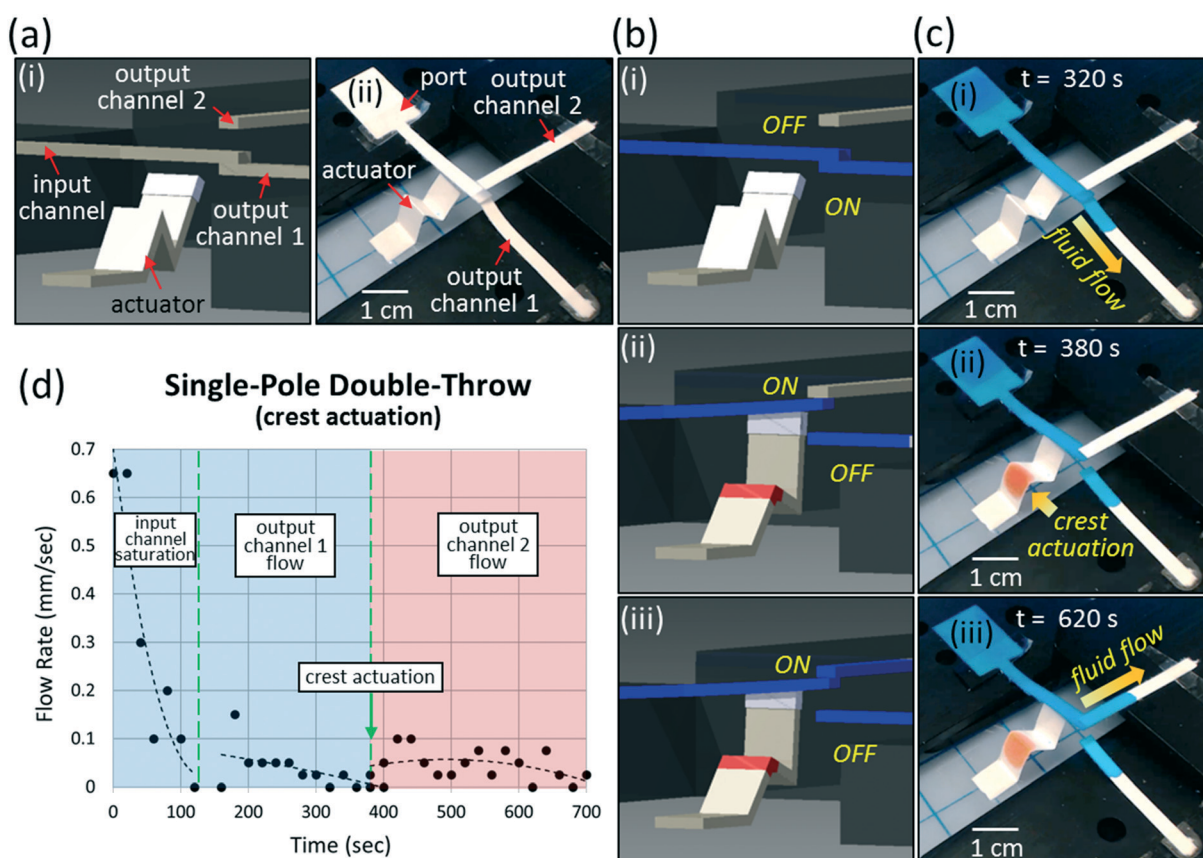

Fig. 5 Single-pole double-throw (SPDT), single-break switch with crest actuation. (a) CAD model (i) and actual image (ii) of the switch are shown. Initially, the input channel is in contact with output channel 1 while output channel 2 is vertically separated from them. An actuator with a single fold is placed such that its tip is positioned vertically below the input channel. (b and c) Figures in panel (b) and panel (c) show the device in CAD model and actual experiment, respectively. Blue-colored water is dropped on the port of the input channel that eventually saturates it and flow is permitted to output channel 1 (b-i and c-i). Red-colored water is then dropped on the crest of the actuator's fold that raises the actuator tip and lifts the input channel to physically separate from output channel 1 and touch output channel 2 (b-ii and c-ii). Fluid flow is now established in output channel 2 (b-iii and c-iii). (d) Flow rate of the fluid front is plotted in the input and output channel 1 before actuation and in the output channel 2 after crest actuation.

actual device). Around 225 μL of blue-colored water is dropped on the port of input channel. Through wicking, the input channel absorbs the blue-colored water and the fluid flows into output channel 1 (Fig. 5b-i and c-i). This configuration represents the ON state for output channel 1 and OFF state for output channel 2. To switch the fluid flow between the two output channels, the actuator is activated by dropping 4 μL of red-colored water on crest of actuator's fold (Fig. 5b-ii and c-ii). The actuator tip lifts the edge of the input channel to separate from output channel 1 while establishing contact with output channel 2. Thereafter, the blue-colored water flows from the input channel to output channel 2 (Fig. 5b-iii and c-iii). This configuration represents the OFF state for output channel 1 and ON state for output channel 2. The flow rate of fluid front in the three channels is plotted in Fig. 5d.

Crest and trough actuation of a single-fold actuator. In previous examples of our toggle switches (Fig. 3–5), wetting the crest of the actuator's folded section lifted its tip to regulate

fluid flow from the input channel to the output channel(s). We also found that wetting the trough of the actuator's folded section lowered its tip. As shown in Fig. 6, the choice of differential wetting of the crest or trough can be employed to turn on and switch fluid flow from the input channel to output channels. The input channel is vertically placed between the two output channels with a physically separation (1 mm) between all the channels. An actuator with a single fold is placed vertically below (1 mm) the input channel. The CAD model and actual device are shown in Fig. 6a-i and a-ii, respectively. Around 225 μL of blue-colored water is dropped on the port of input channel. Through wicking, the input channel absorbs the blue-colored water but there is no fluid flow into the output channels (Fig. 6b-i and c-i). This configuration represents the OFF state for both the output channels. By dropping 4 μL of red-colored water on the crest of the actuator's fold, the tip is lifted to establish contact between the input channel and output channel 1 (Fig. 6b-ii and c-ii). This configuration represents the ON state for output channel 1 and OFF state for output channel
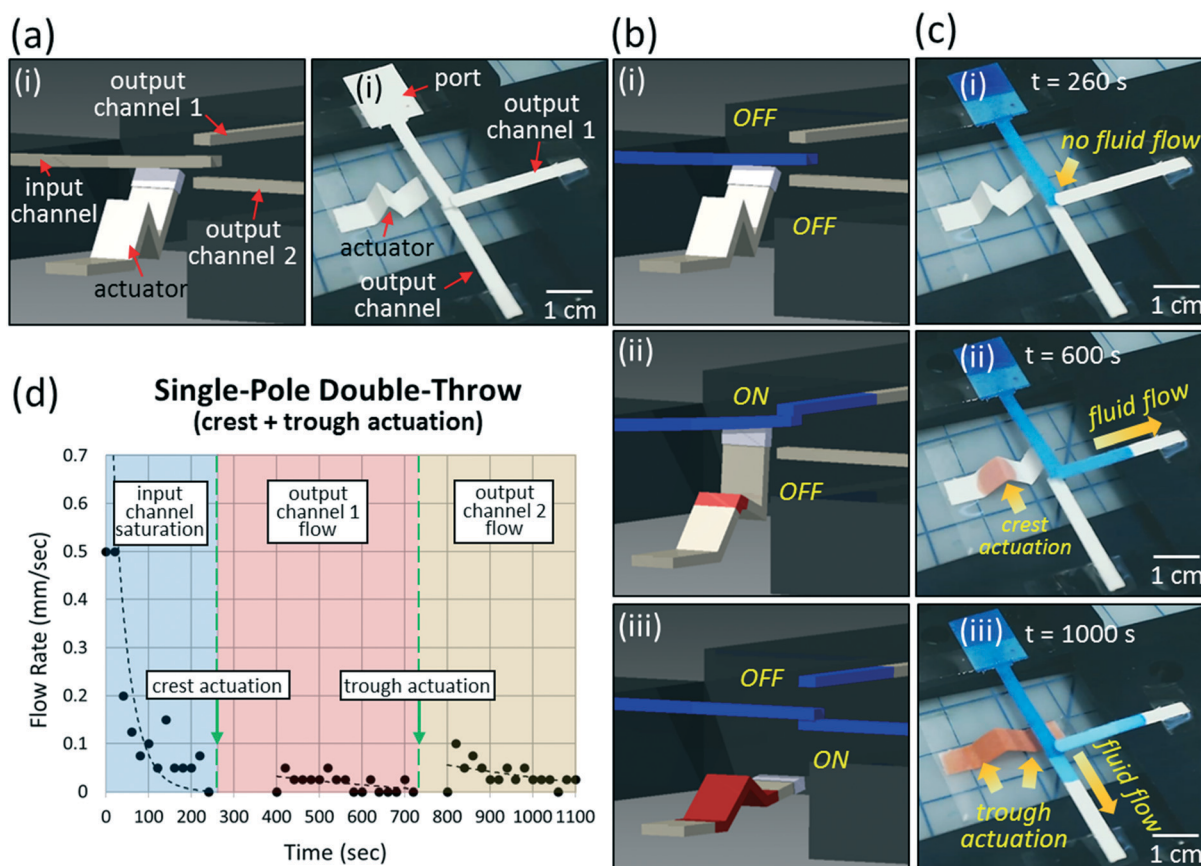

Fig. 6 Single-pole double-throw (SPDT), single-break switch with crest and trough actuation. (a) CAD model (i) and actual image (ii) of the switch are shown. Initially, the input channel is placed in between the two output channels and vertically separated from them. An actuator with a single fold is placed such that its tip is positioned vertically below the input channel. (b and c) Figures in panel (b) and panel (c) show the device in CAD model and actual experiment, respectively. Blue-colored water is dropped on the port of the input channel that eventually saturates it (b-i and c-i). No fluid flow is permitted in the two output channels because of their physical separation from the input channel. Red-colored water is then dropped on the crest of the actuator's fold that raises its tip and brings the input channel in contact with output channel 1 and the blue-colored water now flows into this output channel (b-ii and c-ii). Another round of red-colored water is dropped near the trough of the actuator's fold that lowers the actuator tip and brings the input channel in contact with output channel 2 (b-iii and c-iii). (d) Flow rate of the fluid front is plotted in the input channel before actuation, in output channel 1 after crest actuation, and in output channel 2 after trough actuation.
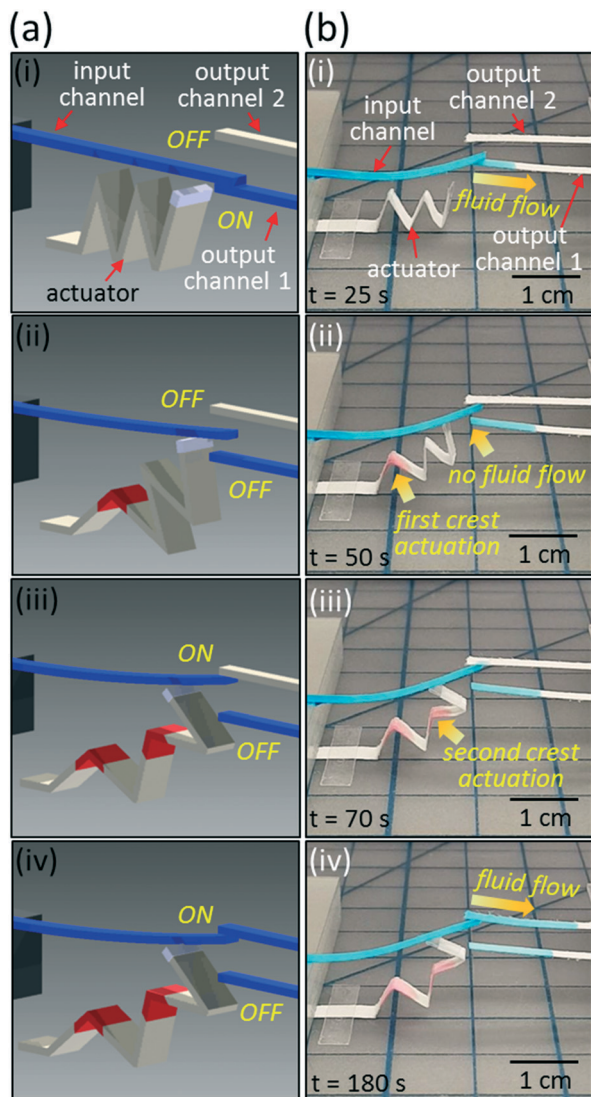
Fig. 7 Single-pole double-throw (SPDT), single-break switch with actuation of two crests. (a and b) Figures in panel (a) and panel (b) depict the device in CAD model and actual experiment, respectively. Initially, the input channel touches output channel 1 but is vertically separated from output channel 2. An actuator with two folds is placed such that its tip is positioned vertically below the input channel. Blue-colored water is dropped on the port of the input channel that eventually saturates it and flow is permitted to output channel 1 (a-i and b-i). Red-colored water is then dropped on the crest of the actuator's left fold that raises the actuator tip and lifts the input channel to physically separate from output channel 1 (a-ii and b-ii). Another round of red-colored water is dropped on the crest of the actuator's right fold that brings the input channel in contact with output channel 2 (a-iii and b-iii). Fluid flow is now established into output channel 2 (a-iv and b-iv).

2. By dropping another 4 μL of red-colored water on the right trough of the actuator's fold, the tip drops down and the input channel makes contact with the output channel 2 placed vertically below it. Fluid flows from the input channel to output channel 2 (Fig. 6b-iii and c-iii). This configuration represents the OFF state for output channel 1 and ON state for output channel 2. The flow rate of fluid front in the three channels is plotted in Fig. 6d.

Two crests' actuation of a multiple-fold actuator. The basic concept of raising the actuator tip by wetting the crest is extended to structures having multiple folds where flow between vertically-aligned channels is controlled by the sequential wetting of individual folds. Fig. 7 demonstrates the switching procedure where the left panel (Fig. 7a) and right panel (Fig. 7b) represent images from the CAD model and actual device, respectively. Initially, the input channel is placed in contact with output channel 1 while output channel 2 is separated by a vertical distance (4 mm) from them. An actuator with two folds is
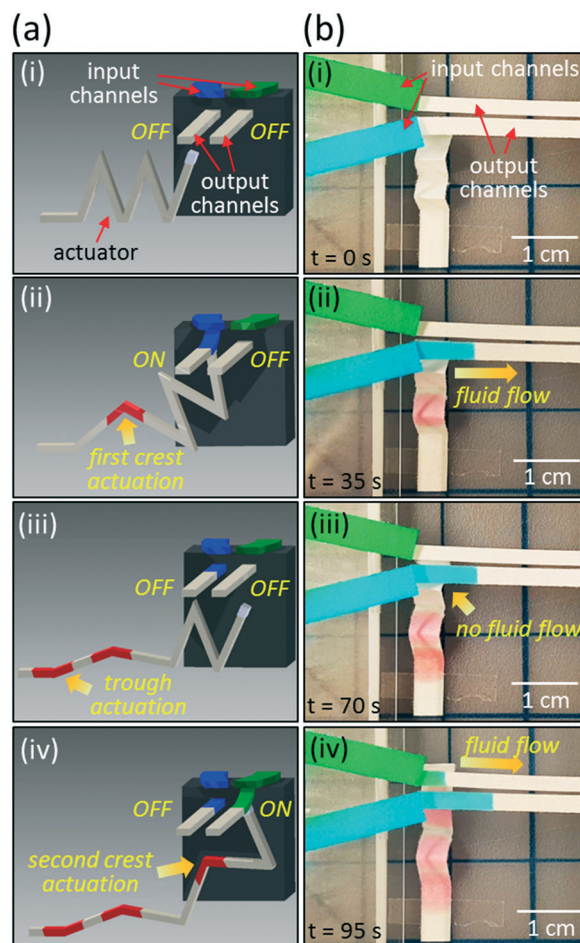

Fig. 8 Single-pole double-throw (SPDT), double-break switch to control two pairs of input and output channels. (a and b) Figures in panel (a) and panel (b) depict the device in CAD model and actual experiment, respectively. Initially, two input channels are placed vertically above their respective output channels but are vertically separated from their output channels. An actuator with two folds is placed such that its tip is positioned vertically below the left input channel. Blue-colored and green-colored water are dropped on the ports of the two input channels which eventually saturate them. Fluid flow is blocked to the output channels (a-i and b-i). Red-colored water is then dropped on the crest of the actuator's left fold that raises the actuator tip and lifts the (left) input channel to touch the (left) output channel (a-ii and b-ii). Another round of red-colored water is dropped on the trough of the actuator's left fold that lowers the tip and removes the previously established connection (a-iii and b-iii). Final round of red-colored water dropped on the crest of the actuator's right fold brings the (right) input channel in contact with the (right) output channel (a-iv and b-iv).
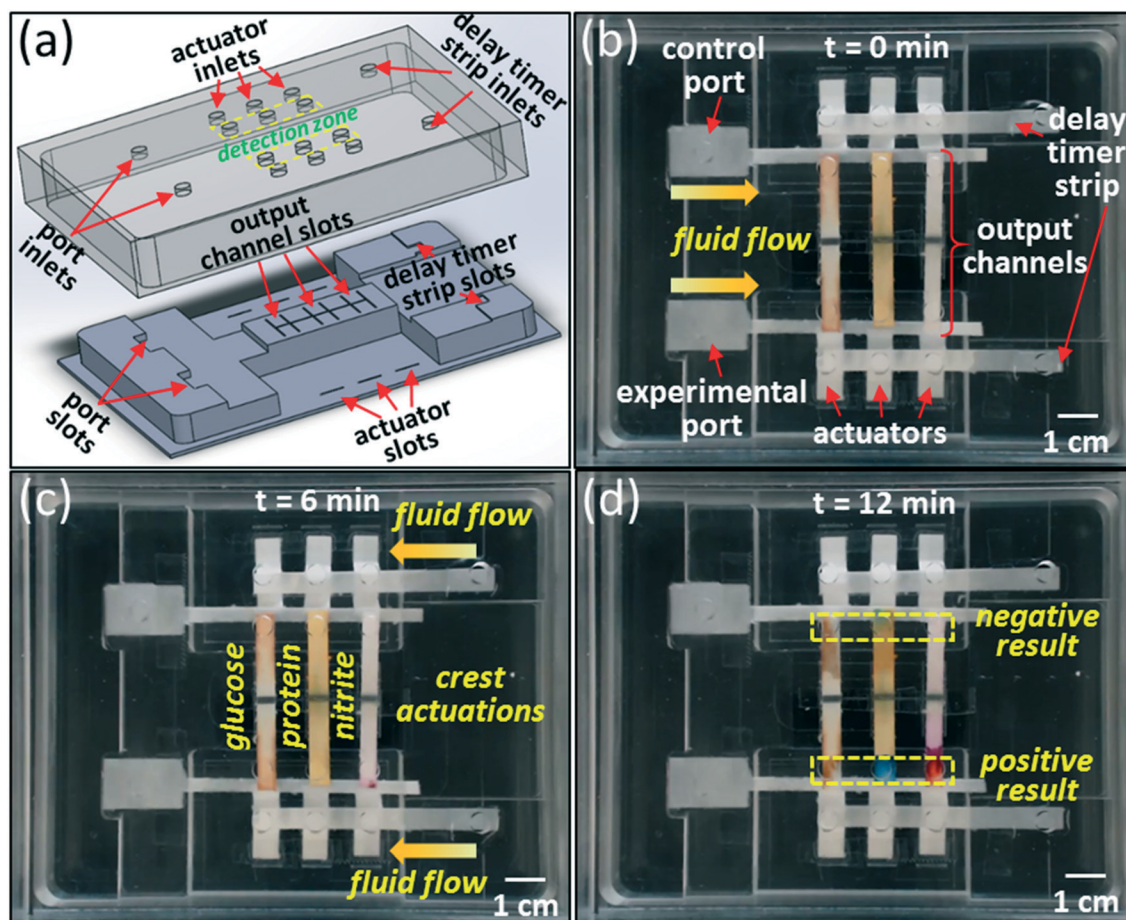
Fig. 9 Colorimetric assay for the simultaneous detection of glucose, protein, and nitrite from artificial saliva. (a) The two-part mold design for the enclosure setup consists of a base and a cover. The base contains slots to place the two input channels, six output channels, six actuators, and two delay timer strips. The cover contains inlets to drop the test and control samples, three reagents, and actuation fluid. The output channels are wicked with the three reagents and dried at room temperature. The channels, actuators, and delay timer strips are taped in their respective slots. (b) Artificial saliva spiked with analytes is dropped on the experimental port while unspiked artificial saliva is used at the control port. By wicking, fluid flows and saturates the two input channels. (c) After a pre-defined delay, distilled water is dropped on the delay time strips. As water travels through a timer strip, the crests of three actuators are activated to raise their respective tips. Thereafter, the experimental fluid flows into the bottom three output channels while the control fluid flows into the top three output channels. (d) A positive color change is confirmed for the experimental case indicating the presence of glucose, protein, and nitrite. A negative color change is shown in the control case.

placed vertically below (1 mm) the input channel. Around 225 μL of blue-colored water is dropped on the port of input channel. Through wicking, the input channel absorbs the blue-colored water and flows into output channel 1 (Fig. 7a-i and b-i). This configuration represents the ON state for output channel 1 and OFF state for output channel 2. The actuator is activated by dropping 4 μL of red-colored water on the crest section of its left fold. This raises the actuator tip and dislodges the input channel from output channel 1. In this configuration, both output channels are in the OFF state (Fig. 7a-ii and b-ii). By dropping another 4 μL of red-colored water on the crest section of the actuator's right fold, the actuator tip lifts up and forces the input channel to make contact with output channel 2 placed vertically above it (Fig. 7a-iii and b-iii). At this instance, fluid flows from the input channel to output channel 2 (Fig. 7a-iv and b-iv). This configuration represents the OFF state for output channel 1 and ON state for output channel 2.

Single-pole double-throw (SPDT), double-break switch

The device comprises four channels (two input channels and two output channels). Initially, both input channels are placed above their respective output channels and separated by a horizontal distance (2 mm). An actuator with two folds is placed vertically below (1 mm) the left input channel. Fig. 8 demonstrates the switching procedure where the left panel (Fig. 8a) and right panel (Fig. 8b) represent images from the CAD model and actual device, respectively. Around 225 μL of blue-colored water and 225 μL of green-colored water are dropped on ports of the two input channels. Through wicking, the input channels absorb the colored water but both output channels are in the OFF state due to the physical separation from their respective input channels (Fig. 8a-i and b-i). Next, 4 μL of red-colored water is dropped on the crest section of the left fold which lifts the actuator tip and

brings the blue-colored input channel in contact with its output channel (Fig. 8a-ii and b-ii). Another 4 μL of red-colored water is dropped on the trough of the left fold which causes the actuator tip to drop and dislodge from the blue-colored output channel (Fig. 8a-iii and b-iii). In this configuration, both output channels are in the OFF state. By dropping 4 μL of red-colored water on the crest of the right fold, the actuator tip is raised. This engages the green-colored input channel to its output channel and enables fluid flow at the juncture (Fig. 8a-iv and b-iv).

Simultaneous detection of glucose, protein, and nitrite from artificial saliva

As a proof-of-concept application, we demonstrate a functional assay to detect the presence of three analytes (*i.e.* glucose, nitrite, and protein) in artificial saliva. A delay timer strip controls the wetting of three actuators, thereby enabling fluid flow from the input channel to three output channels. Two parallel tests (*i.e.* control and experimental) are conducted in the assay. A Plexiglas enclosure setup is constructed to hold the paper strips and provide access points to the user (Fig. 9a). The base of the enclosure (11 cm × 13.5 cm × 1.6 cm) contains slots to hold the two input channels (*i.e.* control and experimental inputs) and six output channels (*i.e.* one pair each of three test strips). In addition, there are slots for six actuators where each actuator connects an input channel to three output channels. For timed programming of actuation, two delay timer strips are used that activate the two sets of three actuators. The cover of the enclosure contains access holes to drop fluid sample and reagents on the respective paper strips.

The output channels are saturated with the three test reagents and allowed to dry at room temperature. One end of all the paper strips (*i.e.* channels, actuators, and delay timer strips) is taped in their allocated slots. Spiked artificial saliva (250 μL) is dropped in the experimental port while unspiked artificial saliva (250 μL) is used in the control port. By wicking, fluid flows in the two input channels until saturation which takes around 6 minutes (Fig. 9b). Thereafter, distilled water is dropped on the ports of the two delay timer strips (Fig. 9c). The actual delay and flow rate in the timer strips can be manipulated by their geometry and surface chemistry. As water travels through a timer strip, the three actuator crests are wetted and activated which, in turn, lifts the input channel to make contact with the three output channels. After chemical reactions occur in the reagent strips, color changes are observed in the detection (Fig. 9d). The positive color changes indicate the presence of three analytes in spiked artificial saliva. Control test strips do not show the intended color change. The sequence of operations during the experiment are attached (video S2†).

In another application, we demonstrate the use of paper actuators with fluidic systems incorporating user-defined delays. A motorized droplet actuation system[64] controls the movement of three discrete droplets (15 μL) on hydrophilic

symbols printed on a super-hydrophobic plastic sheet. Each droplet has a distinct pH value (pH = 8.0, pH = 5.5, and pH = 7.0 (control)). Three pH test paper strips are placed next to the motorized actuation system and supported by three SPST (normally OFF) switches. Upon tilting the stage of the motorized actuation system in sequential steps, each droplet reaches its respective pH test paper strip and is absorbed by actuating the trough of the paper actuator. The time delays in droplet movement and absorption in the pH test paper strip are controlled by the motorized actuation system and paper-based switches, respectively. The produced color changes of the pH test paper strips are compared with the manufacturer's reference table to infer the droplets' pH levels (Fig. S1†).

Conclusion

We demonstrated a reconfigurable actuator device for paper microfluidics to regulate fluid flow between input channel(s) and output channel(s). The actuator is made of paper and requires no extra fabrication steps, coatings, materials or electrical/magnetic stimulation. The actuation principle relies on selectively wetting the crease of a previously-folded paper strip which, in turn, relaxes the crease and increases its fold angle. The actuation height achieved by wetting the crest and trough of the actuator's fold is measured to be 6.9 ± 0.5 mm and 3.8 ± 0.2 mm, respectively. The actuator's response time is within 2 seconds of wetting. A number of switch configurations are realized using the folded paper actuator, such as single-pole single-throw (normally OFF and normally ON) and single-pole double-throw (with single and double break). A colorimetric assay is presented where the presence of glucose, protein, and nitrite are detected in spiked artificial saliva. The assay integrates the parallel operations of multiple actuators, delay timer strips, and flow channels in a portable enclosure. The advantages of this actuation method include easy preparation steps by paper cutting and folding, very fast actuator response time, choice between different switch configurations, no observable contamination of the flow channels by the actuation fluid, ability to integrate and scale multiple actuators, and significantly reduced cost of materials and labor.

Conflicts of interest

There are no conflicts of interest to declare.

Acknowledgements

References

1 W. Martinez, S. T. Phillips, M. J. Butte and G. M. Whitesides, *Angew. Chem., Int. Ed.*, 2007, **46**, 1318–1320.

2 W. Martinez, S. T. Phillips and G. M. Whitesides, *Proc. Natl. Acad. Sci. U. S. A.*, 2008, **105**, 19606–19611.

3 W. Martinez, S. T. Phillips, Z. Nie, C.-M. Cheng, E. Carrilho, B. J. Wiley and G. M. Whitesides, *Lab Chip*, 2010, **10**, 2499–2504.

4 W. Martinez, S. T. Phillips, G. M. Whitesides and E. Carrilho, *Anal. Chem.*, 2010, **82**, 3–10.

5 B. Li, W. Zhang, L. Chen and B. Lin, *Electrophoresis*, 2013, **34**, 2162–2168.

6 K. Yetisen, M. S. Akram and C. R. Lowe, *Lab Chip*, 2013, **13**, 2210–2251.

7 R. Park, *Lateral-flow POC tests to grow*, http://ivdtechnology. com/article/lateral-flow-poc-tests-grow, (accessed June 2013).

8 G. A. Posthuma-Trumpie, J. Korf and A. Amerongen, *Anal. Bioanal. Chem.*, 2009, **393**, 569–582.

9 R. Wong and H. Tse, *Lateral Flow Immunoassay*, Humana Press, Totowa, NJ, 2009.

10 T. Acharya, A. S. Daar, E. Dowdeswell, P. A. Singer and H. Thorsteinsdottir, *Genomics and Global Health, University of Toronto Joint Centre for Bioethics*, Toronto, Ontario, Canada, 2004.

11 G. M. Carr and J. P. Neary, *Water Quality for Ecosystem and Human Health*, GEMS/Water Programme, Burlington, Ontario, Canada, 2008.

12 WHO, *Global Strategy for Food Safety: Safer Food for Better Health*, F. S. Department, Food Safety Department, WHO, Geneva, Switzerland, 2002.

13 WHO, *Foodborne Disease Outbreaks: Guidelines for Investigation and Control*, WHO, France, 2008.

14 J. Saldanha, A. Parashar, S. Pandey and J. Powell-Coffman, *Toxicol. Sci.*, 2013, **135**(1), 156–168.

15 A. Beeman, Z. Njus, S. Pandey and G. Tylka, *Phytopathology*, 2016, **106**(12), 1563–1571.

16 E. Fu and C. Downs, *Lab Chip*, 2017, **17**, 614–628.

17 X. Li, D. R. Ballerini and W. Shen, *Biomicrofluidics*, 2012, **6**, 11301–1130113.

18 D. R. Ballerini, X. Li and W. Shen, *Microfluid. Nanofluid.*, 2012, **13**, 769–787.

19 D. D. Liana, B. Raguse, J. J. Gooding and E. Chow, *Sensors*, 2012, **12**, 11505–11526.

20 C. Parolo and A. Merkoci, *Chem. Soc. Rev.*, 2013, **42**, 450–457.

21 P. Shah, X. Zhu and C. Z. Li, *Expert Rev. Mol. Diagn.*, 2013, **13**, 83–91.

22 T. Kong, R. Brien, Z. Njus, U. Kalwa and S. Pandey, *Lab Chip*, 2016, **16**(10), 1861–1872.

23 *In vitro Diagnostics (IVD) Market (Applications, End-users & Types) Trends & Global Forecasts (Major & Emerging Markets - G7, Japan & BRIC)*, Markets and Markets, 2011, http://www.marketsandmarkets.com/Market-Reports/in-vitro-diagnostics-ivd-market-547.html, (accessed September 2017).

24 J. Marchant, *Innovations in Diagnostics (Next Generation Molecular & Point of Care Diagnostics Driving Personalised Healthcare)*, Business Insights Ltd, 2006.

25 E. Fu, P. Yager, P. N. Floriano, N. Christodoulides and J. Mcdevitt, *IEEE Pulse*, 2011, **2**, 40–50.

26 B. J. Toley, J. A. Wang, M. Gupta, J. R. Buser, L. K. Lafleur, B. R. Lutz, E. Fu and P. Yager, *Lab Chip*, 2015, **15**, 1432–1444.

27 J. Carr, R. Lycke, A. Parashar and S. Pandey, *Appl. Phys. Lett.*, 2011, **98**(14), 143701.

28 S. Pandey, A. Joseph, R. Lycke and A. Parashar, *Adv. Biosci. Biotechnol.*, 2011, **2**, 409–415.

29 R. Lycke, A. Parashar and S. Pandey, *Biomicrofluidics*, 2013, **7**(6), 064103.

30 K. N. Han, J. S. Choi and J. Kwon, *Sci. Rep.*, 2016, **6**, 25710.

31 B. D. Grant, C. A. Smith, K. Karvonen and R. Richards-Kortum, *Anal. Chem.*, 2016, **88**, 2553–2557.

32 S. Ramachandran, E. Fu, B. Lutz and P. Yager, *Analyst*, 2014, **139**, 1456–1462.

33 J. Saldanha, S. Pandey and J. Powell-Coffman, *Life. Sci. Space Res.*, 2016, **10**, 38–46.

34 R. Gerbers, W. Foellscher, H. Chen, C. Anagnostopoulos and M. Faghri, *Lab Chip*, 2014, **14**, 4042–4049.

35 E. W. Washburn, *Phys. Rev.*, 1921, **17**, 273–283.

36 R. Lucas, *Kolloid-Z.*, 1918, **23**, 15–22.

37 S. Mendez, E. M. Fenton, G. R. Gallegos, D. N. Petsev, S. S. Sibbett, H. A. Stone, Y. Zhang and G. P. Lopez, *Langmuir*, 2010, **26**, 1380–1385.

38 E. Fu, B. Lutz, P. Kauffman and P. Yager, *Lab Chip*, 2010, **10**, 918–920.

39 A. C. Glavan, R. V. Martinez, E. J. Maxwell, A. B. Subramaniam, R. M. D. Nunes, S. Soh and G. M. Whitesides, *Lab Chip*, 2013, **13**, 2922–2930.

40 C. Renault, X. Li, S. E. Fosdick and R. M. Crooks, *Anal. Chem.*, 2013, **85**, 7976–7979.

41 D. L. Giokas, G. Z. Tsogas and A. G. Vlessidis, *Anal. Chem.*, 2014, **86**, 6202–6207.

42 H. Noh and S. T. Phillips, *Anal. Chem.*, 2010, **82**, 8071–8078.

43 C. H. Weng, M. Y. Chen, C. H. Shen and R. J. Yang, *Biomicrofluidics*, 2014, **8**, 066502.

44 B. Lutz, T. Liang, E. Fu, S. Ramachandran, P. Kauffman and P. Yager, *Lab Chip*, 2013, **13**, 2840–2847.

45 B. J. Toley, B. McKenzie, T. Liang, J. R. Buser, P. Yager and E. Fu, *Anal. Chem.*, 2013, **85**, 11545–11552.

46 E. Fu, T. Liang, P. Spicar-Mihalic, J. Houghtaling, S. Ramachandran and P. Yager, *Anal. Chem.*, 2012, **84**, 4574–4579.

47 K. N. Han, J. S. Choi and J. Kwon, *Sci. Rep.*, 2016, **6**, 25710.

48 C. Koo, F. He and S. Nugen, *Analyst*, 2013, **138**, 4998–5004.

49 L. F. Cai, M. H. Zhong, H. L. Li, C. X. Xu and B. Y. Yuan, *Biomicrofluidics*, 2015, **9**, 046503.

50 Y. Jiang, Z. X. Hao, Q. H. He and H. W. Chen, *RSC Adv.*, 2016, **6**, 2888–2894.

51 L. K. Lafleur, J. D. Bishop, E. K. Heiniger, R. P. Gallagher, M. D. Wheeler, P. Kauffman, X. H. Zhang, E. C. Kline, J. R. Buser, S. Kumar, S. A. Byrnes, N. M. J. Vermeulen, N. K. Scarr, Y. Belousov, W. Mahoney, B. J. Toley, P. D. Ladd, B. R. Lutz and P. Yager, *Lab Chip*, 2016, **16**, 3777–3787.

52 J. Houghtaling, T. Liang, G. Thiessen and E. Fu, *Anal. Chem.*, 2013, **85**, 11201–11204.

53 B. R. Lutz, P. Trinh, C. Ball, E. Fu and P. Yager, *Lab Chip*, 2011, **11**, 4274–4278.

54 X. Li, P. Zwanenburg and X. Liu, *Lab Chip*, 2013, **13**, 2609–2614.

55 H. Liu and R. M. Crooks, *J. Am. Chem. Soc.*, 2011, **133**, 17564–17566.

56 W. Liu, C. L. Cassano, X. Xu and Z. H. Fan, *Anal. Chem.*, 2013, **85**, 10270–10276.

57 K. J. Paz-Alfaroa, Y. G. Ruiz-Granadosb, S. Uribe-Carvajalb and J. G. Sampedro, *J. Biotechnol.*, 2009, **141**, 130–136.

58 J. Sun, X. Zhang, M. Broderick and H. Fein, *Sensors*, 2003, **3**, 276–284.

59 M. M. Bradford, *Anal. Biochem.*, 1976, **72**, 248–254.

60 B. B. Kim, H. A. Kadir and S. Tayyab, *Pak. J. Biol. Sci.*, 2008, **11**(20), 2418–2422.

61 A. C. Khazraji and S. Robert, *J. Nanomater.*, 2013, **2013**, 409676.

62 E. Reyssat and L. Mahadevan, *Europhys Lett.*, 2011, **93**, 54001.

63 B. Thiria and M. Adda-Bedia, *Phys. Rev. Lett.*, 2011, **107**, 025506.

64 T. Kong, R. Brien, Z. Njus, U. Kalwa and S. Pandey, *Lab Chip*, 2016, **16**, 1861.